Grant Agreement No.: 779606

Project acronym: EVERYWH2ERE

Project title: Making Hydrogen affordable to sustainably operate Everywhere in European cities

Call (part) identifier: H2020-JTI-FCH-2017-1

Thematic Priority: FHC-02-10-2017, Transportable FC gensets for temporary power supply in urban applications

Starting date of project: 1st February, 2018

Duration: 60 months

Project URL: www.everywh2ere.eu

WP2 – System Integration and 25 kW Prototype Realization

D2.3 – Optimized design of an ejector to be integrated in the 25 kW EVERYWH2ERE genset

Due date of deliverable	
31st July, 2019	
Actual submission date	**Deliverable version**
30th September 2019	1.0

Organisation name of lead contractor for this deliverable: VTT

Dissemination Level		
CO	Confidential	
PU	Public	**X**

This project has received funding from the Fuel Cells and Hydrogen 2 Joint Undertaking under grant agreement No 779606. This Joint Undertaking receives support from the European Union's Horizon 2020 research and innovation programme, Hydrogen Europe and Hydrogen Europe research.

Executive Summary

EVERYWH2ERE "D2.3 – Optimized design of an ejector to be integrated in the 25 kW EVERYWH2ERE genset" describes the design of a dual-ejector system to be integrated in the 25 kW genset. The work conducted can be bundled in three parts. First, the experimental characterization of a modular ejector is reported. The experimental data serves as a reference for assessing the validity of simulation results. Second, the modelling approach is presented and simulation results are benchmarked against experimental data. The sizing of dual-ejector relies on modelling. Third and finally, the dual-ejector sizing methods and results are presented.

This project has received funding from the Fuel Cells and Hydrogen 2 Joint Undertaking under grant agreement No 779606. This Joint Undertaking receives support from the European Union's Horizon 2020 research and innovation programme, Hydrogen Europe and Hydrogen Europe research.

Table of Contents

This project has received funding from the Fuel Cells and Hydrogen 2 Joint Undertaking under grant agreement No 779606. This Joint Undertaking receives support from the European Union's Horizon 2020 research and innovation programme, Hydrogen Europe and Hydrogen Europe research.

List of Figures

This project has received funding from the Fuel Cells and Hydrogen 2 Joint Undertaking under grant agreement No 779606. This Joint Undertaking receives support from the European Union's Horizon 2020 research and innovation programme, Hydrogen Europe and Hydrogen Europe research.

This project has received funding from the Fuel Cells and Hydrogen 2 Joint Undertaking under grant agreement No 779606. This Joint Undertaking receives support from the European Union's Horizon 2020 research and innovation programme, Hydrogen Europe and Hydrogen Europe research.

Abbreviations and acronyms

FC	Fuel cell stack
CFD	Computational Fluid Dynamics
NTP	Normal temperature (273.15 K = 0 °C) and pressure (1.01325 bara)
nlpm	Normal litres per minute
PLC	Programmable Logic Controller
D_m	Ejector mixing section diameter [mm] or [x D_{nt}]
D_{nt}	Ejector nozzle throat diameter [mm]
D_{no}	Ejector nozzle outlet diameter [mm] or [x D_{nt}] (convergent-divergent nozzles)
L_m	Ejector mixing section length [mm] or [x D_{nt}]
L_{ne}	Distance between nozzle tip and mixing section in ejector [mm] or [x D_{nt}]
$\dot{m}_{p,in}$	Ejector primary gas mass flow rate [kg/s]
$\dot{m}_{s,in}$	Ejector secondary gas mass flow rate [kg/s]
$\dot{F}_{p,in}$	Ejector primary gas volumetric flow rate at NTP [nlpm]
$\dot{m}_{e,out}$	Ejector outlet gas mass flow rate [kg/s]
$p_{FC,in}$	Fuel cell inlet pressure [barg]
$p_{FC,out}$	Fuel cell outlet pressure [barg]
$p_{p,in}$	Ejector primary inlet pressure [barg]
$p_{s,in}$	Ejector secondary inlet pressure [barg]
$p_{e,out}$	Ejector outlet pressure [barg]
Δp_e	Ejector pressure difference (= $p_{e,out} - p_{s,in}$) [bar]
Δp_{FC}	Fuel cell pressure drop (= $p_{FC,in} - p_{FC,out}$) [bar]
α_d	Ejector diffuser divergence angle [°]
α_{pd}	Ejector nozzle divergence angle [°] (convergent-divergent nozzles)
λ	Hydrogen stoichiometry at anode inlet [-]
Ω	Ejector entrainment ratio (= $\dot{m}_{s,in}$ / $\dot{m}_{p,in}$) [-]

This project has received funding from the Fuel Cells and Hydrogen 2 Joint Undertaking under grant agreement No 779606. This Joint Undertaking receives support from the European Union's Horizon 2020 research and innovation programme, Hydrogen Europe and Hydrogen Europe research.

1. Introduction

This public report is part of H2020-FCH-JU project "EVERYWH2ERE - Making Hydrogen affordable to sustainably operate Everywhere in European cities" and it was prepared within the framework of Work Package 2.

EVERYWH2ERE aims to demonstrate the reliability of using FC technologies in temporary power gensets replacing current state-of-the-art solutions mostly based on diesel engines, thus opening a niche but relevant market for FC technologies. During the whole project 8 PEMFC (4x25 kw and 4x100 kW) equipped containered "plug and play" gensets will be realized and tested through a pan-European demonstration campaign in a demonstration to market approach. The prototypes will be tested in construction sites, music festivals and urban public events all around Europe, demonstrating their flexibility and their.enlarged lifetime. Demonstration results will be widely promoted and they will be helpful for the promotion of replicability studies (for the use of gensets in further end-user contexts) and for the definition of a commercial roadmap and suitable business model for the complete marketability of the gensets within 2025

This deliverable was prepared within the framework of Work Package 2: System Integration and 25 kW Prototype Realization, and it covers the description and results of designing an optimized duel-ejector system for the 25 kW genset.

Ejectors are pumps that have no moving parts – the pumping effect is achieved by accelerating a high-pressure fluid to high velocity, which then entrains a fluid at lower pressure. Because of the absence of moving parts, ejectors are robust and inexpensive. This makes them well suited for improving fuel cell system efficiency, reliability and decreasing system cost. The control of ejector can be made fast so that is not limiting ramp rate of the fuel cell system [1].

Ejector sizing is a complex task. To date, there are no universally accepted sizing methods. Often, methods relying on Computational Fluid Dynamics (CFD, a numerical modelling approach) or on semi-empiric 0-dimensional mathematical modelling are employed.

Whatever the sizing method, it involves an iterative process for continuously verifying (and improving) the result experimentally. This process is depicted in Figure 1.

This project has received funding from the Fuel Cells and Hydrogen 2 Joint Undertaking under grant agreement No 779606. This Joint Undertaking receives support from the European Union's Horizon 2020 research and innovation programme, Hydrogen Europe and Hydrogen Europe research.

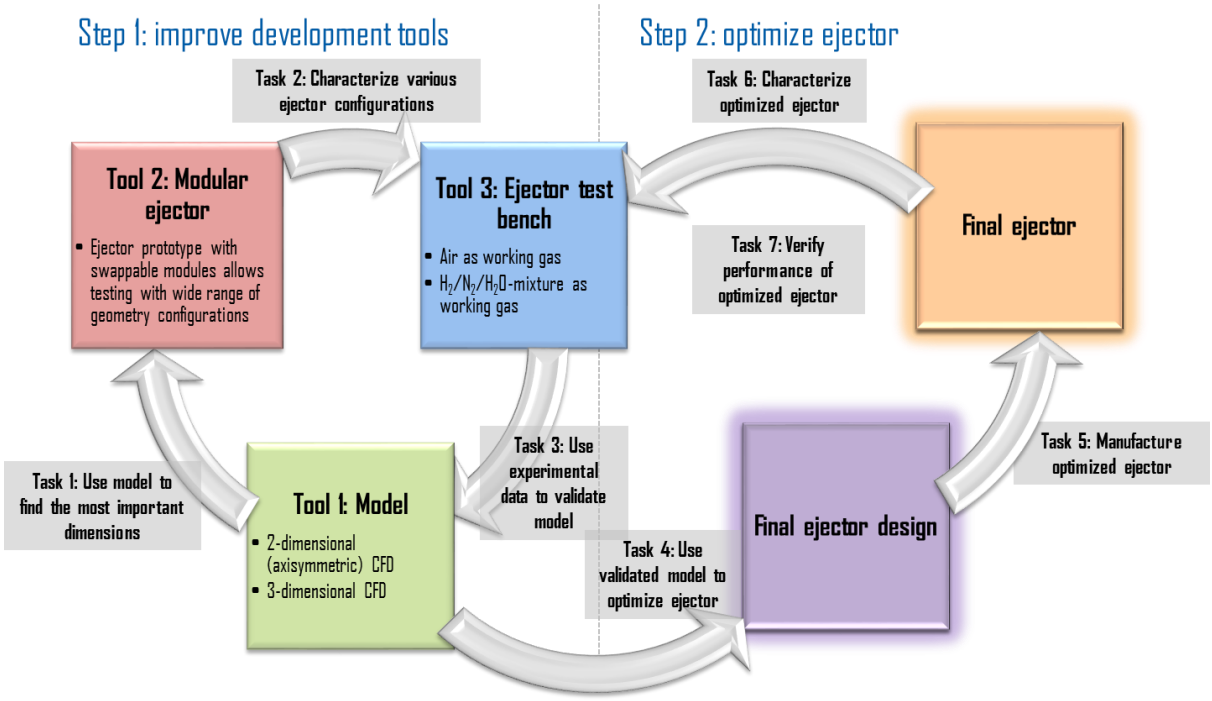

Figure 1. Optimization of ejector with three tools: 1) a CFD model, 2) a modular ejector, and 3) an ejector test bench.

The process depicted in Figure 1 is also executed in the work that is described in this document. Based on previous simulations and experiments [2,3], a modular ejector has been designed. In this work, the various modifications of the modular ejector are characterized experimentally. This experimental data serves as a reference for assessing the validity of simulation results. A validated modelling tool gives more confidence for optimization. Ultimately, the performance of the optimized ejector should be verified experimentally.

This project has received funding from the Fuel Cells and Hydrogen 2 Joint Undertaking under grant agreement No 779606. This Joint Undertaking receives support from the European Union's Horizon 2020 research and innovation programme, Hydrogen Europe and Hydrogen Europe research.

2. Ejector experimental characterization

2.1 Methods

The experimental characterization of ejectors is conducted by testing several configurations of a modular ejector in a test bench that was designed and built for the purpose. Both the modular ejector and the test bench has been designed and built within the MARANDA-project (Grant agreement no: 735717). Descriptions of the modular ejector, the test bench, and the experimental approach follows.

Modular ejector

The idea with a modular ejector is that a large number of ejector designs can be characterized with a small number of parts. This not only is economical but also beneficial from manufacturing tolerance point of view. In manufacturing ejectors (or ejector parts in this case), manufacturing tolerances are always present. Unless very small, the tolerances may cause the ejector performance to deviate from the intended. Hence, employing a modular ejector design for characterization eliminates the unintended differences between various configurations and visualizes more clearly the true effect of the changed dimension.

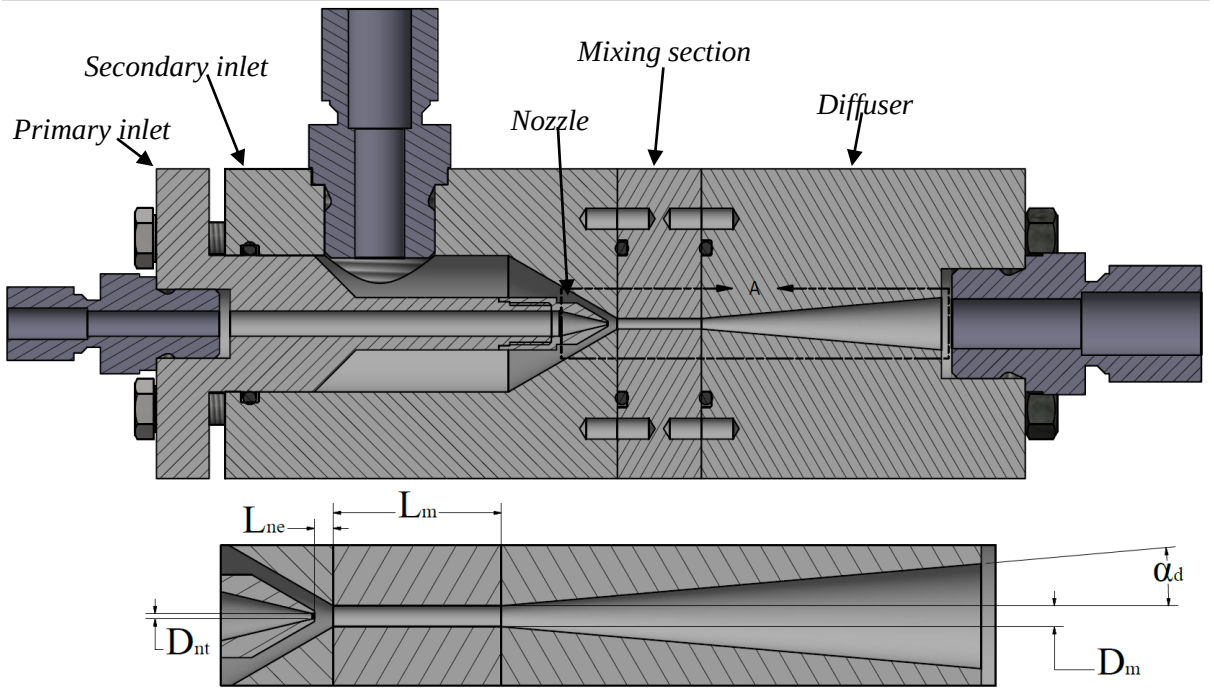

Figure 2. Side-cut view of the modular ejector design.

Figure 2 shows the modular ejector employed in this work. The ejector consists of five parts (or modules): 1) primary inlet, 2) secondary inlet, 3) nozzle, 4) mixing section, and 5) diffuser. There parts are interchangeable with some limitations. For example, the length of the mixing section (L_m) or the diverging angle of the diffuser (α_d) can be studied by keeping rest of the ejector dimensions unchanged. Moreover, the axial position of the primary inlet (and, hence,

This project has received funding from the Fuel Cells and Hydrogen 2 Joint Undertaking under grant agreement No 779606. This Joint Undertaking receives support from the European Union's Horizon 2020 research and innovation programme, Hydrogen Europe and Hydrogen Europe research.

the nozzle can be varied. This enables to study the effect of nozzle position relative to mixing section (L_{ne}). Finally, the diameter of the mixing section (D_m) can also be varied but in this case, also the secondary inlet and diffuser must be replaced with ones that match openings to the mixing section. Figure 3 shows a photo of some of the parts available and Table 1 list s all parts currently available.

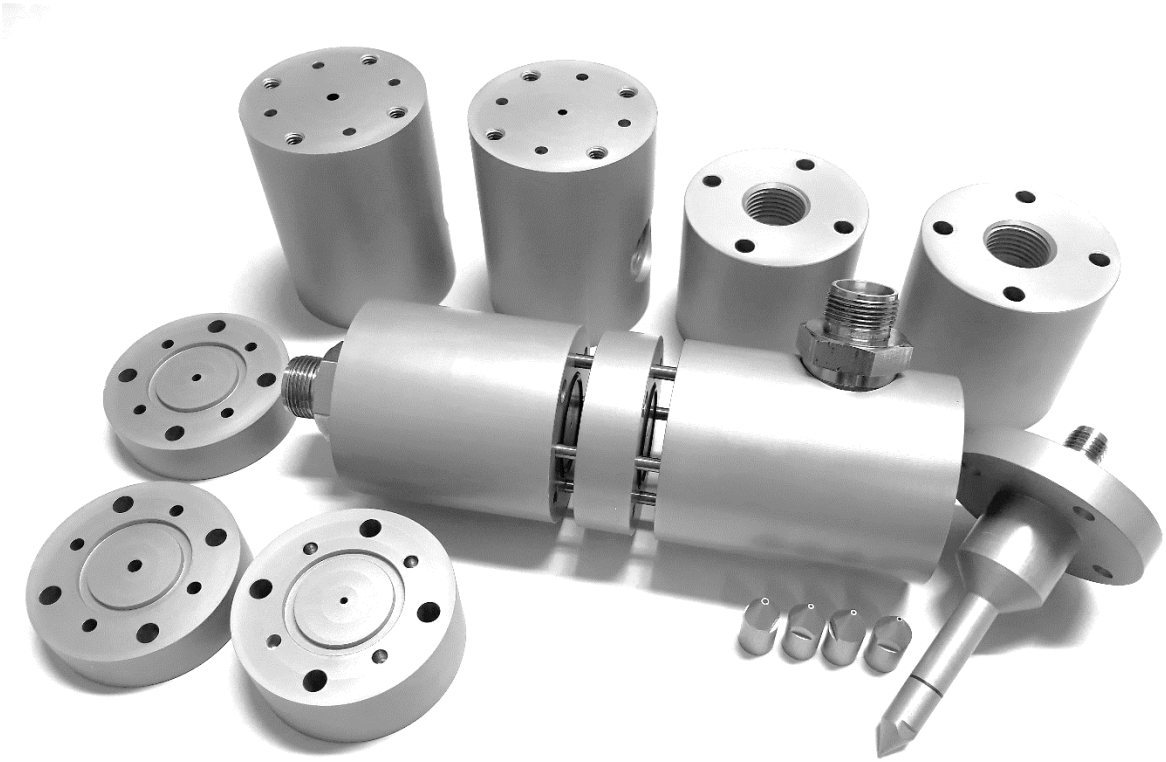

Figure 3. A photo of modular ejector parts.

Table 1. List of all parts currently available.

Part [#]	***D_{nt}***	***D_{no}***		***D_m***		***L_m***		***α_d***
	[mm]	*[mm]*	*[x D_{nt}]*	*[mm]*	*[x D_{nt}]*	*[mm]*	*[x D_{nt}]*	*[°]*
Nozzles								
1	0.5	0.5	1					
2	0.5	1.0	2					
3	0.5	1.5	3					
4	0.5	1.0	2					
5	0.5	1.0	2					
Secondary inlets								
1				2.0	4			
2				3.0	6			
3				4.0	8			
Mixing sections								
1				2.0	4	*16*	*32*	

This project has received funding from the Fuel Cells and Hydrogen 2 Joint Undertaking under grant agreement No 779606. This Joint Undertaking receives support from the European Union's Horizon 2020 research and innovation programme, Hydrogen Europe and Hydrogen Europe research.

2			3.0	6	*16*	*32*	
3			4.0	8	*16*	*32*	
4			2.0	4	*8*	*16*	
5			2.0	4	*24*	*48*	
Diffusers							
1			2.0	4			5
2			3.0	6			5
3			4.0	8			5

In this work, the number of varied ejector dimensions is limited to three: the distance between nozzle and the mixing section (L_{ne}), the mixing section diameter (D_m), and the mixing section length (L_m). These were found to affect ejector performance the most when performing a preliminary study by modelling. Table 2 lists the ejector configurations characterized in this work.

Table 2. Ejector configurations characterized in this work.

Ejector	D_{nt}	L_{ne}	D_m	L_m	α_d
#	[mm]	[mm]	[mm]	[mm]	[°]
1	0.5	1.88	2.0	16	5
2	0.5	0.88	2.0	16	5
3	0.5	2.88	2.0	16	5
4	0.5	3.88	2.0	16	5
5	0.5	1.88	3.0	16	5
6	0.5	1.88	4.0	16	5
7	0.5	1.88	2.0	8	5
8	0.5	1.88	2.0	24	5

Test bench

A PLC-controlled ejector test bench has been designed and built at VTT within the MARANDA-project. The test bench is suited to characterize ejectors sized for ca 20 kW fuel cell systems with hydrogen and ca 80 kW with air. The pressure at the ejector inlets and outlet can be controlled independently and the secondary inlet gas can be humidified if desired. Moreover, the nitrogen content of the secondary gas is controllable. So, the actual operating conditions in a fuel cell system can be emulated accurately. Figure 4 shows a simplified schematic of the test bench and Figure 5 shows a photo of it.

This project has received funding from the Fuel Cells and Hydrogen 2 Joint Undertaking under grant agreement No 779606. This Joint Undertaking receives support from the European Union's Horizon 2020 research and innovation programme, Hydrogen Europe and Hydrogen Europe research.

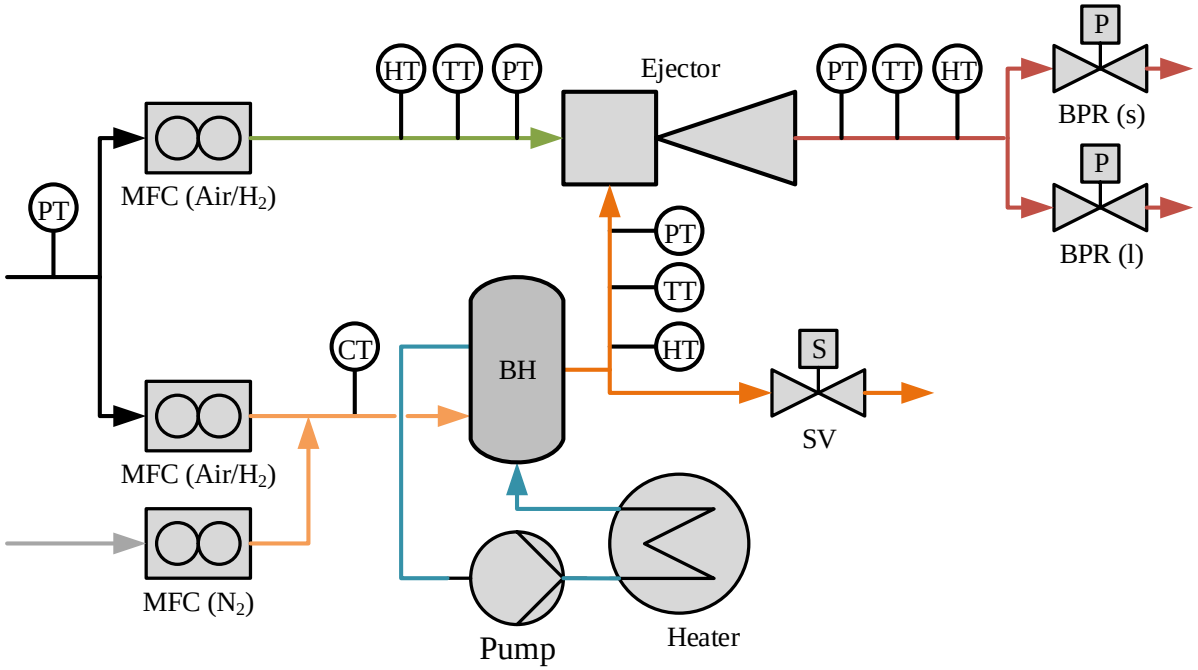

Figure 4. Simplified test bench schematic. MFC: mass flow controller, MH: membrane humidifier, BPR: backpressure regulator (s: small, l: large), TT: temperature transmitter, PT: pressure transmitter, HT: humidity transmitter, CT: H_2 concentration transmitter, SV: safety valve.

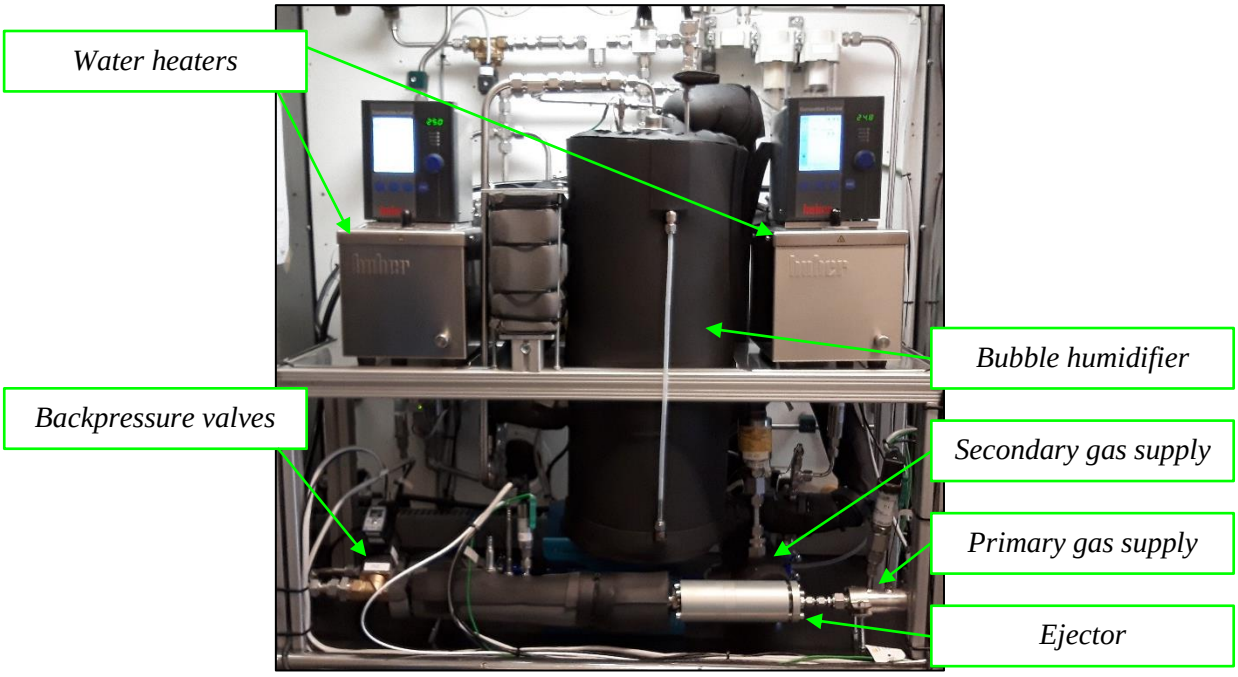

Figure 5. A photo of ejector test bench at VTT.

This project has received funding from the Fuel Cells and Hydrogen 2 Joint Undertaking under grant agreement No 779606. This Joint Undertaking receives support from the European Union's Horizon 2020 research and innovation programme, Hydrogen Europe and Hydrogen Europe research.

Experimental approach

The experiments were conducted at four conditions listed in Table 3. They are not exactly those specified for the target system in EVERYWH2ERE-project since the same experiments will be used in the MARANDA-project.

Table 3. Conditions for ejector characterization.

$\dot{F}_{p,in}$ [nlpm]	$p_{s,in}$ [barg]	$p_{e,out}$ [barg]	$y_{H2,s,in}$ [-]	$y_{N2,s,in}$ [-]	$y_{H2O,s,in}$ [-]	$T_{s,in}$ [°C]
13.8	0.5	0.5 … max (4)	0.55	0.24	0.21	70
27.8	0.8	0.8 … max (4)	0.58	0.25	0.17	70
47.6	1.2	1.2 … max (4)	0.60	0.26	0.14	70
71.3	1.2	1.2 … max (4)	0.60	0.26	0.14	70

At the condition with primary gas flow rate ($\dot{F}_{p,in}$) set to 13.8 nlpm, the primary pressure ($p_{p,in}$) is ca 1.0 barg and the primary flow in the nozzle is subcritical. With $\dot{F}_{p,in}$ set to 27.8 nlpm, the primary pressure is ca 2.5 barg and the flow is just above the critical limit. The primary gas flow rates of 47.6 nlpm and 71.3 nlpm correspond to primary pressures of ca 5.0 barg and 8.0 barg, respectively. At both conditions, the primary flow is well above the critical limit.

At each condition, the secondary inlet pressure ($p_{s,in}$) is maintained constant while the ejector outlet pressure ($p_{e,out}$) is varied. The notation '0.5 … max (4)' means that the outlet pressure is varied at four levels between 0.5 barg and the maximum pressure. The maximum outlet pressure is the pressure where the secondary flow is zero. In other words, it is the maximum pressure against which the ejector can operate at such conditions.

The secondary inlet gas at each condition is saturated with water at 70 °C the rest being hydrogen and nitrogen. The dry gas nitrogen mole fraction is 30%.

The measurements were conducted by first measuring the maximum ejector outlet pressures for each ejector configuration. This was done by plugging the secondary inlet and controlling the ejector outlet pressure to a level where the target secondary inlet pressure was achieved. The measurement was ran into steady state and maintained there for at least two minutes – one for stabilization and one for averaging data. In these measurements, the conditions at the secondary inlet were naturally not those listed in Table 3.

When the maximum outlet pressure for all ejector configurations were known, the secondary flow rate at the minimum outlet pressure were measured while maintaining the secondary gas composition as listed in Table 3. The minimum outlet pressure equals the secondary inlet pressure, which essentially means that the ejector operates against no pressure head. At this condition, the secondary flow rate reaches its maximum (as is the case with rotating pumps). Finally, the two remaining outlet pressures were recorded by setting the secondary flow rate a value between zero and the maximum value just determined.

This project has received funding from the Fuel Cells and Hydrogen 2 Joint Undertaking under grant agreement No 779606. This Joint Undertaking receives support from the European Union's Horizon 2020 research and innovation programme, Hydrogen Europe and Hydrogen Europe research.

With the approach presented here, the characteristic curves of the ejector operated at different primary pressure levels are obtained. These correspond the characteristic curves of rotating pumps operated at different rotating speeds.

The control of secondary inlet humidity level was slow because of the relatively large thermal mass (the heating water and the water contained in the bubble humidifier). Therefore, the strategy with humid gas measurements was to slowly approach the target conditions and record one minute of data (for averaging) as close as the target as possible.

2.2 Results

Effect of the distance between nozzle exit and mixing section

In this report the ejector performance is expressed as λ-Δp_e –curves, which is a form of a characteristic curve. An ejector λ-Δp_e –curve is a plot of the recirculation rate (in terms of anode inlet stoichiometry per pass) that the ejector can achieve as function of pressure head (i.e. the difference of ejector outlet pressure and ejector secondary inlet pressure, $\Delta p_e = p_{e,out} - p_{s,in}$). In a practical fuel cell system the pressure head (Δp_e) is the pressure drop in the anode side of the stack.

Figure 6 shows the ejector performance as λ-Δp_e –curves that were measured with varying distance between nozzle exit and mixing section (L_{ne}).

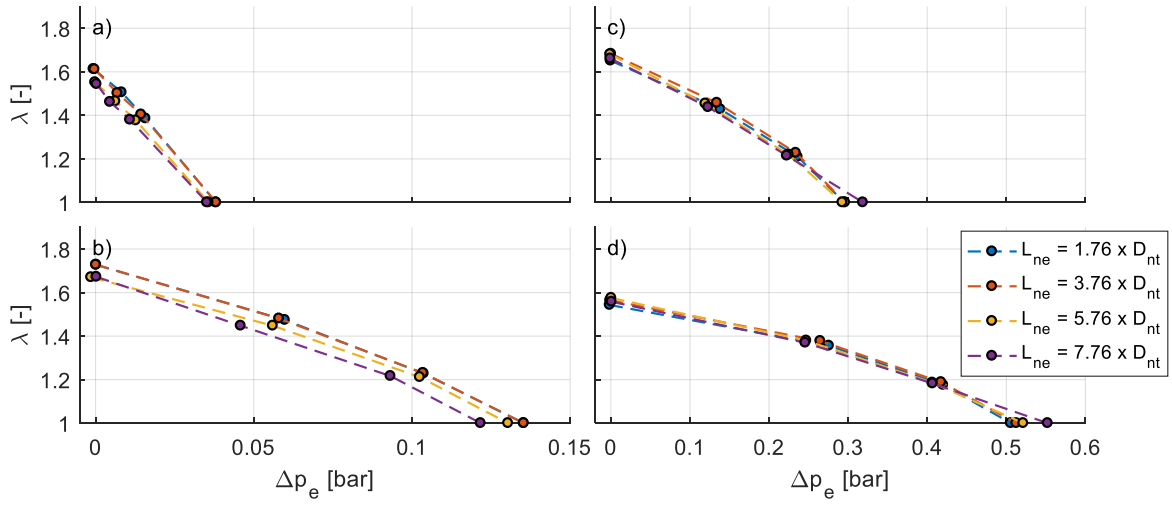

Figure 6. Ejector λ-Δp_e –curves with varying distance between nozzle exit and mixing section (L_{ne}) at 4 primary pressure levels a) $p_{p,in}$ = 1.0 barg, b) $p_{p,in}$ = 2.5 barg, c) $p_{p,in}$ = 4.9 barg, d) $p_{p,in}$ = 7.8 barg. D_m = 4 x D_{nt}, L_m = 32 x D_{nt}.

The ejector λ-Δp_e –curves show that the achieved recirculation rate increases with decreasing L_{ne}, especially at low primary pressure levels ($p_{p,in}$ = 1.0 barg and $p_{p,in}$ = 2.5 barg). At higher primary pressure levels ($p_{p,in}$ = 4.9 barg and $p_{p,in}$ = 7.8 barg), the effect is less pronounce but also then the ejector with the longest distance between the nozzle and the mixing section (L_{ne} = 7.76 x D_{nt}) generally performs worst.

This project has received funding from the Fuel Cells and Hydrogen 2 Joint Undertaking under grant agreement No 779606. This Joint Undertaking receives support from the European Union's Horizon 2020 research and innovation programme, Hydrogen Europe and Hydrogen Europe research.

The results also suggest that the maximum pressure head (with zero secondary flow rate) achieved with an ejector decreases with L_{ne} at low primary pressures (Figure 6a and Figure 6b) but increases with L_{ne} at high primary pressures (Figure 6c and Figure 6d). However, this might also be a result of measurement inaccuracies.

It is useful to plot how each of the ejectors would work in the real FC system with the expected conditions. Figure 7 shows the recirculation rate achieved using ejectors with varying L_{ne} in the target system (assuming that the system is operated at the conditions of ejector experiments in Table 3). Again, the highest performance is achieved with smallest L_{ne} at low stack current levels whereas, at high current levels, the optimal L_{ne} increases. An ejector with L_{ne} = 3.76 x D_{nt} performs well both at low and high stack current levels. This result already illustrates that high λ over all the operating range is difficult to achieve with a single ejector.

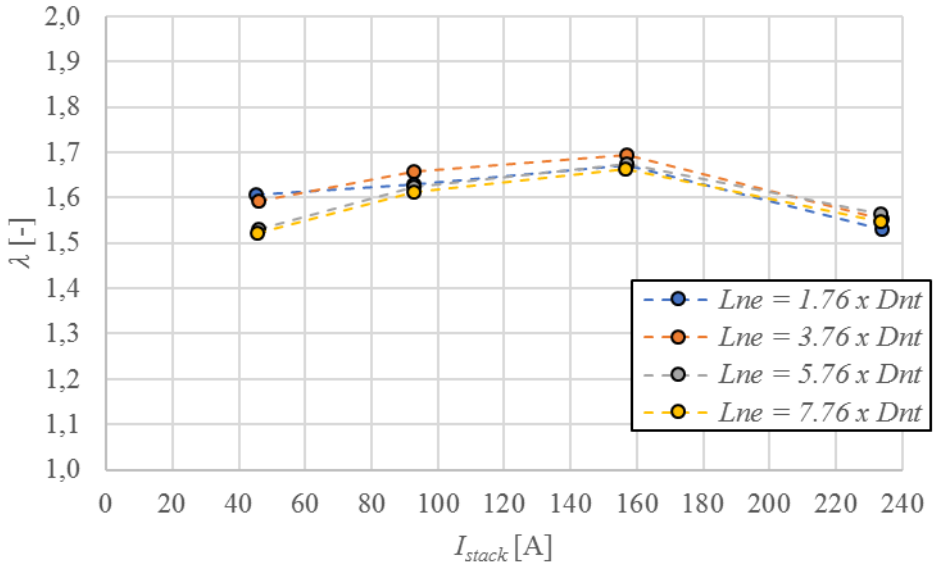

Figure 7. Effect of distance between nozzle exit and mixing section (L_{ne}) on anode inlet stoichiometric ratio of hydrogen (λ) in the target fuel cell system. The experimentally measured recirculation rate is fitted into quadratic polynomials that are solved with the target system flow resistance. D_m = 4 x D_{nt}, L_m = 32 x D_{nt}.

Effect of mixing section diameter

Figure 8 shows the ejector λ-Δp_e –curves that were measured with varying mixing section diameter (D_m). The results show that the maximum recirculation rate (with Δp_e = 0) increases with increasing D_m, whereas the maximum pressure head (with zero secondary flow rate) increases with decreasing D_m. This is true for all primary pressure levels.

This project has received funding from the Fuel Cells and Hydrogen 2 Joint Undertaking under grant agreement No 779606. This Joint Undertaking receives support from the European Union's Horizon 2020 research and innovation programme, Hydrogen Europe and Hydrogen Europe research.

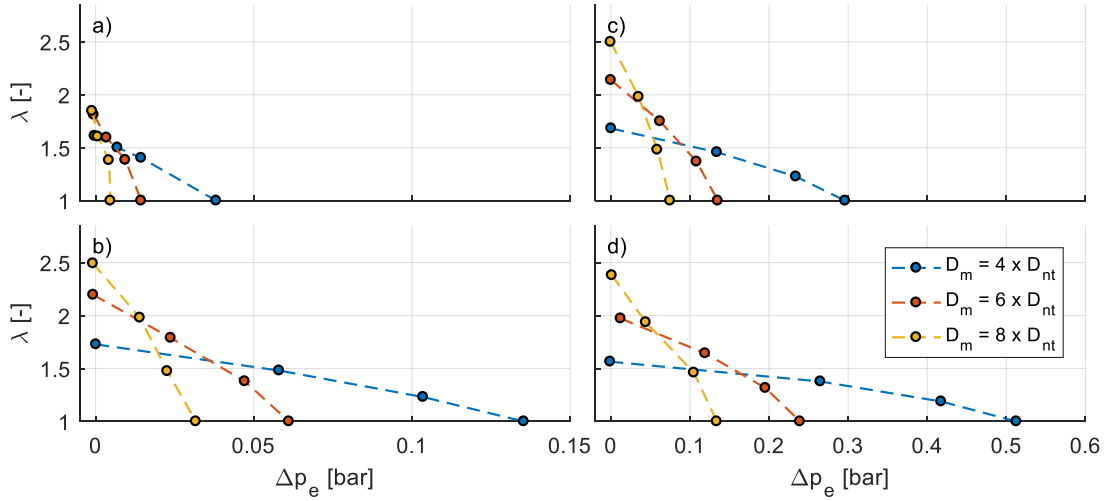

Figure 8. Ejector λ-Δp_e –curves with varying mixing section diameter (D_m) at 4 primary pressure levels a) $p_{p,in}$ = 1.0 barg, b) $p_{p,in}$ = 2.5 barg, c) $p_{p,in}$ = 4.9 barg, d) $p_{p,in}$ = 7.8 barg. L_{ne} = 3.76 x D_{nt}, L_m = 32 x D_{nt}.

The D_m has a notably stronger effect on ejector performance than the distance between nozzle exit and mixing section (L_{ne}) and, as will be seen later, mixing section length (L_m). Hence, if only one dimension would be optimized, D_m would be the choice.

Figure 8 is also useful for visualizing the effect of system flow resistance on the achieved recirculation rate using ejectors with varying D_m. In a system with low flow resistance, the Δp versus recirculation rate is steep and the highest recirculation rate is achieved using an ejector with high D_m. In a system with high flow resistance, the Δp versus recirculation rate is less steep and the highest recirculation rate is achieved using an ejector with low D_m.

Figure 9 shows the recirculation rate achieved using ejectors with varying D_m in the target system (assuming that the system is operated at the conditions of ejector experiments). This figure shows clearly how the optimal ejector dimensions change with stack current level. At low current levels (ca 40 A), both the ejector with D_m = 4 x D_{nt} and the ejector with D_m = 6 x D_{nt} outperform the ejector with D_m = 8 x D_{nt}. However, at higher current levels, the ejector with D_m = 8 x D_{nt} achieves clearly higher recirculation rate than the other two.

This project has received funding from the Fuel Cells and Hydrogen 2 Joint Undertaking under grant agreement No 779606. This Joint Undertaking receives support from the European Union's Horizon 2020 research and innovation programme, Hydrogen Europe and Hydrogen Europe research.

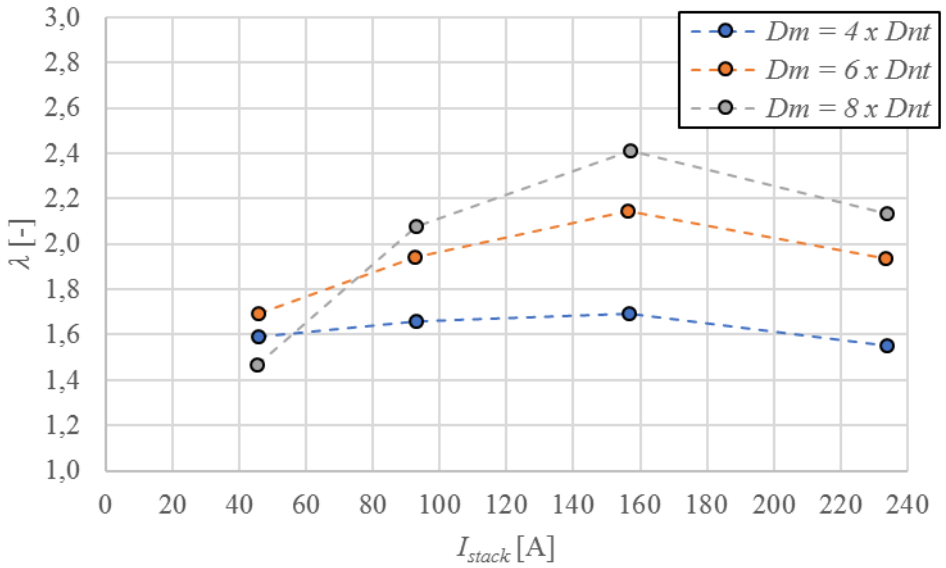

Figure 9. Effect of mixing section diameter (D_m) on anode inlet stoichiometric ratio of hydrogen (λ) in the target fuel cell system. The experimentally measured recirculation rate is fitted into quadratic polynomials that are solved with the target system flow resistance. L_{ne} = 3.76 x D_{nt}, L_m = 32 x D_{nt}.

Effect of mixing section length

Figure 10 shows the ejector λ-Δp_e –curves that were measured with varying mixing section length (L_m). The results show that at low primary pressures ($p_{p,in}$ = 1.0 barg), the highest recirculation rate is achieved with small L_m, (i.e. L_m = 16 x D_{nt} and L_m = 32 x D_{nt}). However, at or above critical primary gas flow (Figure 10b-d), the recirculation rate achieved with L_m = 16 x D_{nt} is notably lower than that achieved with L_m = 32 x D_{nt}. Similarly, above critical primary gas flow conditions (Figure 10c-d), the recirculation rate achieved with L_m = 48 x D_{nt} is same level as that achieved with L_m = 48 x D_{nt}. The ejector with L_m = 32 x D_{nt} achieves high recirculation at both low and high primary pressures.

This project has received funding from the Fuel Cells and Hydrogen 2 Joint Undertaking under grant agreement No 779606. This Joint Undertaking receives support from the European Union's Horizon 2020 research and innovation programme, Hydrogen Europe and Hydrogen Europe research.

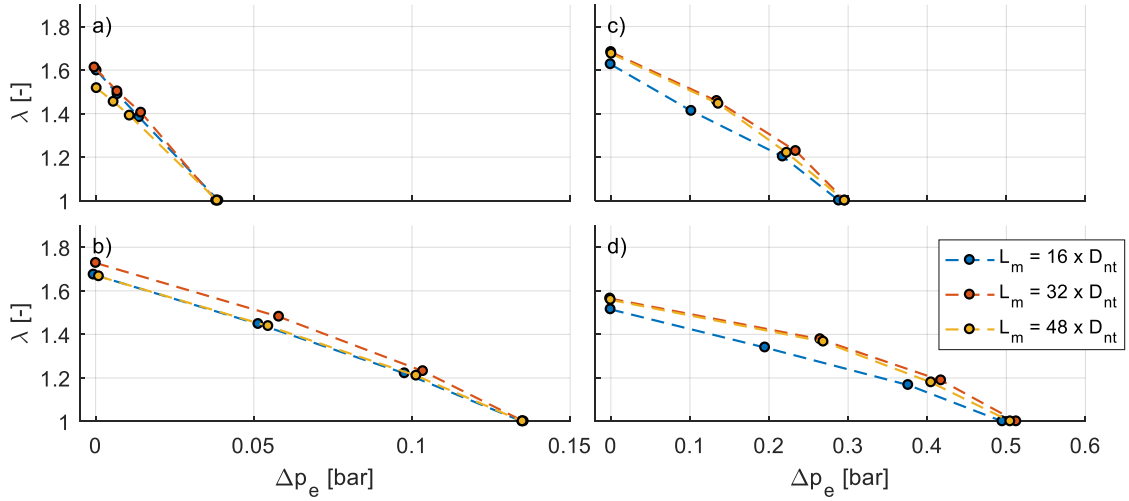

Figure 10. Ejector λ-Δp_e –curves with varying mixing section length (L_m) at 4 primary pressure levels a) $p_{p,in}$ = 1.0 barg, b) $p_{p,in}$ = 2.5 barg, c) $p_{p,in}$ = 4.9 barg, d) $p_{p,in}$ = 7.8 barg. L_{ne} = 3.76 x D_{nt}, D_m = 4 x D_{nt}.

Figure 11 shows the recirculation rate achieved using ejectors with varying L_m in the target system (assuming that the system is operated at the conditions of ejector experiments). This figure confirms the observations made in Figure 10. An ejector with L_m = 16 x D_{nt} achieves high recirculation rate at low primary pressures (low stack current level). An ejector with L_m = 48 x D_{nt} achieves high recirculation rate at high primary pressures (high stack current level). An ejector with L_m = 32 x D_{nt} achieves high recirculation rate at both low and high primary pressures.

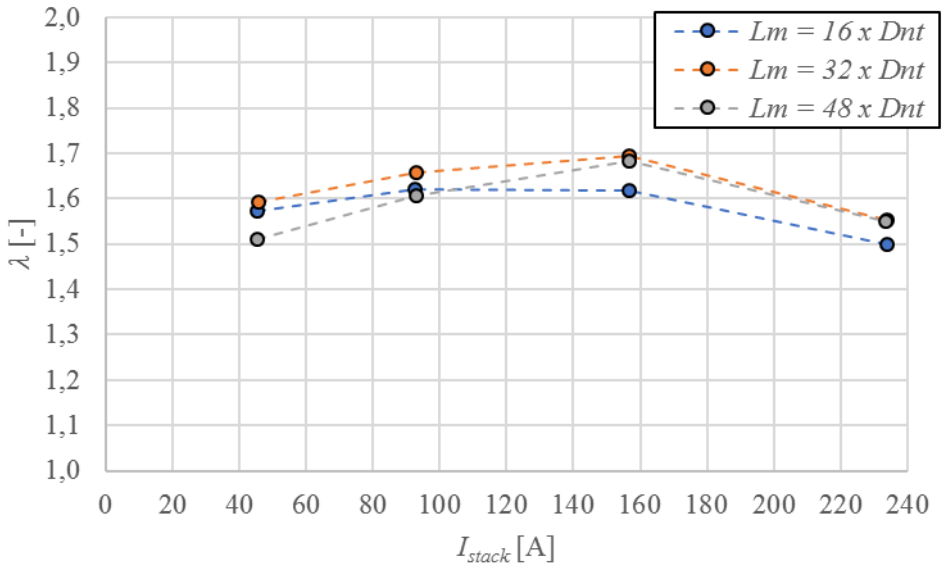

Figure 11. Effect of mixing section length (L_m) on anode inlet stoichiometric ratio of hydrogen (λ) in the target fuel cell system. The experimentally measured recirculation rate is fitted into quadratic polynomials that are solved with the target system flow resistance. L_{ne} = 3.76 x D_{nt}, D_m = 4 x D_{nt}.

This project has received funding from the Fuel Cells and Hydrogen 2 Joint Undertaking under grant agreement No 779606. This Joint Undertaking receives support from the European Union's Horizon 2020 research and innovation programme, Hydrogen Europe and Hydrogen Europe research.

3. Ejector modelling

3.1 Methods

The simulations were conducted using the same approach as described in a previous work [2] with the following exceptions:

- a newer version (19.1) of the Ansys software package was employed
- only the Re-Normalization Group (RNG) k-ε turbulence model was employed
- Ansys DesignModeler was employed for creating parametrized geometries
- Ansys Meshing-tool was employed for creating parametrized quad-dominant meshes with inflation
- Meshes were refined where high gradients of Mach number occurred

The Re-Normalization Group (RNG) k-ε turbulence model was employed because in a previous work [2], it was observed estimate the position of highest ejector performance correctly.

The use of parametrized geometries and meshes enabled simulating a large number of geometries with minimum effort put on drawing and meshing. The parametrized meshing was found particularly useful in mesh independence studies, which were conducted for the simulated ejector geometries.

Dynamic (during simulations) mesh refinement was enabled to perform with 500 iteration intervals. The refinement was performed where high gradients of Mach number occurred. The refinement limit for Mach number was set to 0.0005 because this was observed to be low enough for mesh independent results.

The models were solved with Ansys Fluent. The momentum balance equations and pressure based continuity equation were solved in a coupled manner and the remaining equations (energy conservation, species conservation, and turbulence transport) were solved in a segregated manner. A 2^{nd} order pressure interpolation scheme was employed and all the equations were spatially discretized with 2^{nd} order upwind schemes.

Ejector inlet (both primary and secondary) temperatures, pressures, and gas compositions as well as ejector outlet pressure were used as boundary conditions. The flow directions were assumed normal to inlets with a 5% turbulence intensity. The ejector walls were assumed smooth and adiabatic and the no-slip condition was adopted. The physical properties (heat capacity, diffusion coefficients, viscosity, and thermal conductivity) were computed with correlations presented in previous work [2]. Fluent's Hybrid initialization was employed to obtain an initial solution for the solver.

Because of the parametrized geometries and meshes, the simulation cases could be (and were) organized as design points in Ansys Workbench. A large number (typically hundreds to more than a thousand) design points were then submitted for solution through Ansys Remote Solve Manager (RSM). The actual computation was performed either on a local computer or on

This project has received funding from the Fuel Cells and Hydrogen 2 Joint Undertaking under grant agreement No 779606. This Joint Undertaking receives support from the European Union's Horizon 2020 research and innovation programme, Hydrogen Europe and Hydrogen Europe research.

VTT's computing cluster. The local computer is running Windows 10 Pro and has a Dual Intel Xeon processor (2.2 GHz) with totally 40 computing cores and 128 GB of memory. The remote computing cluster comprises Linux machines based on 2nd to 6th generation Intel microarchitecture (Sandy Bridge to Skylake) each having 16 to 36 computing cores (totally around 3000 cores) and 128 GB to 772 GB memory. Typically, 30 to 100 cores were allocated for solving a range of design points. The total time for all simulations (the sum of all simulation time) were several weeks.

3.2 Results

In this section, the simulation results are compared with experimental results.

Figure 12 shows a comparison of experimental results and simulations on ejector performance when the distance between nozzle exit and mixing section (L_{ne}) is varied. The simulations overestimate the ejector performance quite radically but this was expected based on previous work [2].

The general trend of the effect of L_{ne} is quite well in line with the experiments: the recirculation rate increases with decreasing L_{ne}, especially at low primary pressure levels ($p_{p,in}$ = 1.0 barg and $p_{p,in}$ = 2.5 barg). However, in contrast to observations made from experiments, there seems to an optimum in L_{ne} around 3.76 x D_{nt}. This optimum is at least almost independent of the primary pressure level.

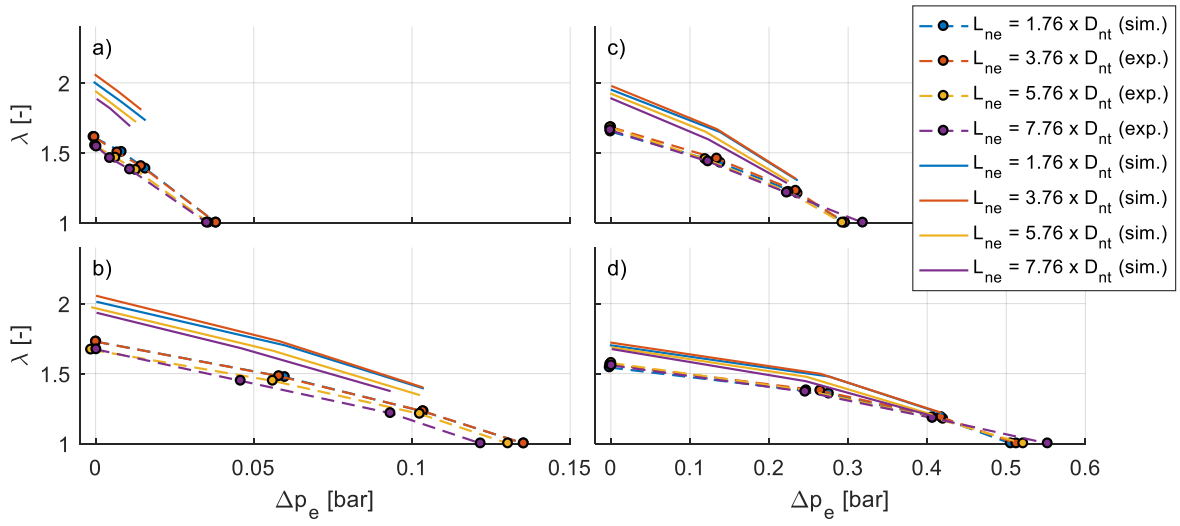

Figure 12. Ejector λ-Δp_e –curves with varying distance between nozzle exit and mixing section (L_{ne}) at 4 primary pressure levels a) $p_{p,in}$ = 1.0 barg, b) $p_{p,in}$ = 2.5 barg, c) $p_{p,in}$ = 4.9 barg, d) $p_{p,in}$ = 7.8 barg. D_m = 4 x D_{nt}, L_m = 32 x D_{nt}. Comparison between experimental results and simulations.

Figure 13 shows a comparison of experimental results and simulations on ejector performance when the mixing section diameter (D_m) is varied. Like above, the simulation results overestimate the ejector performance radically but the general trend seems right. More studies are needed to verify that the trend is correct.

This project has received funding from the Fuel Cells and Hydrogen 2 Joint Undertaking under grant agreement No 779606. This Joint Undertaking receives support from the European Union's Horizon 2020 research and innovation programme, Hydrogen Europe and Hydrogen Europe research.

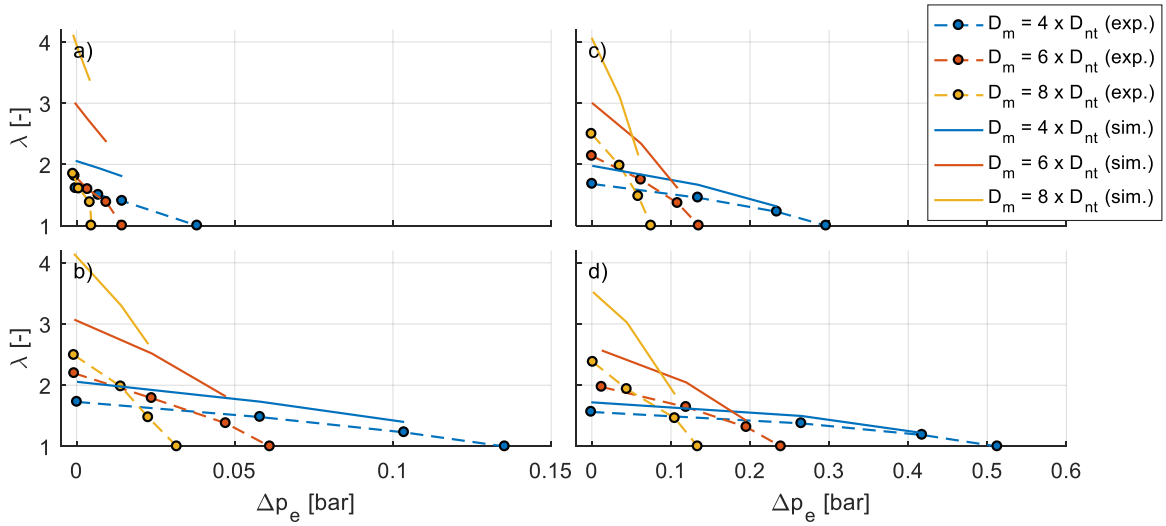

Figure 13. Ejector λ-Δp_e –curves with varying mixing section diameter (D_m) at 4 primary pressure levels a) $p_{p,in}$ = 1.0 barg, b) $p_{p,in}$ = 2.5 barg, c) $p_{p,in}$ = 4.9 barg, d) $p_{p,in}$ = 7.8 barg. L_{ne} = 3.76 x D_{nt}, L_m = 32 x D_{nt}. Comparison between experimental results and simulations.

Figure 14 shows a comparison of experimental results and simulations on ejector performance when the mixing section length (L_m) is varied. Again, the simulation results overestimate the ejector performance radically. In contrast to conclusions made from experimental data, the simulation results suggest that the recirculation rate increases with decreasing L_m. This is true for all primary pressure levels.

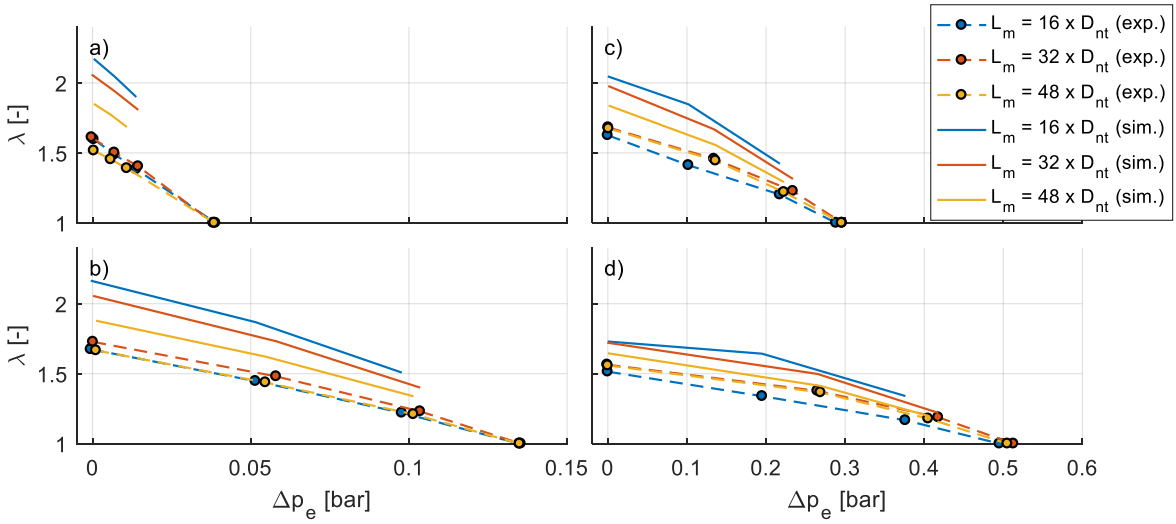

Figure 14. Ejector λ-Δp_e –curves with varying mixing section length (L_m) at 4 primary pressure levels a) $p_{p,in}$ = 1.0 barg, b) $p_{p,in}$ = 2.5 barg, c) $p_{p,in}$ = 4.9 barg, d) $p_{p,in}$ = 7.8 barg. L_{ne} = 3.76 x D_{nt}, D_m = 4 x D_{nt}. Comparison between experimental results and simulations.

In conclusion, the simulation results radically overestimate ejector performance but in general, the trends of varied dimension seem correct. Even though the model is useful for finding the optimum dimensions [2], it gives a bad estimate of the actually achieved recirculation rate. This is true especially for low stack current part, which is unfortunate. When stack current is low the

This project has received funding from the Fuel Cells and Hydrogen 2 Joint Undertaking under grant agreement No 779606. This Joint Undertaking receives support from the European Union's Horizon 2020 research and innovation programme, Hydrogen Europe and Hydrogen Europe research.

humidity is highest, see Table 3, and risk for liquid water accumulation is large. Therefore, ejector should have good performance so that water can be removed from anode channels.

4. Ejector design optimization

4.1 Target fuel cell system specifications

Figure 15 shows schematic diagram of the target fuel cell system. Hydrogen is supplied from storage through a pressure reducer to proportional valves..The proportional valves function as flow controllers for the ejectors so that they can be controlled independently of the other. The ejectors are passive devices that only pass a flow that is proportional to the upstream pressure (i.e. the primary pressure, $p_{p,in}$) and the flow opening (i.e. the nozzle diameter). Inside the ejectors, the high-speed primary flow entrains the low-pressure secondary flow from fuel cell outlet. The primary and secondary flows mix and flow out of the ejector into the fuel cell stack. When returning from the fuel cell stack to the ejector secondary inlets, the anode gas passes check valves. These prevent the anode gas from flowing in the wrong direction when one of the ejectors is idle and the other one is active. Figure 15 represents the final (real) FC system as VTT imagine it also according to PCS indications. The proportional valves upstream of the ejectors are needed to control the primary pressures of the ejectors. The pressure regulator in Figure 15 outputs a nearly constant pressure (10 barg) but the primary pressure (1.7-7.5 barg) applied to the ejectors depend on the stack current level. The proportional valves can be replaced with some other pressure regulating devices

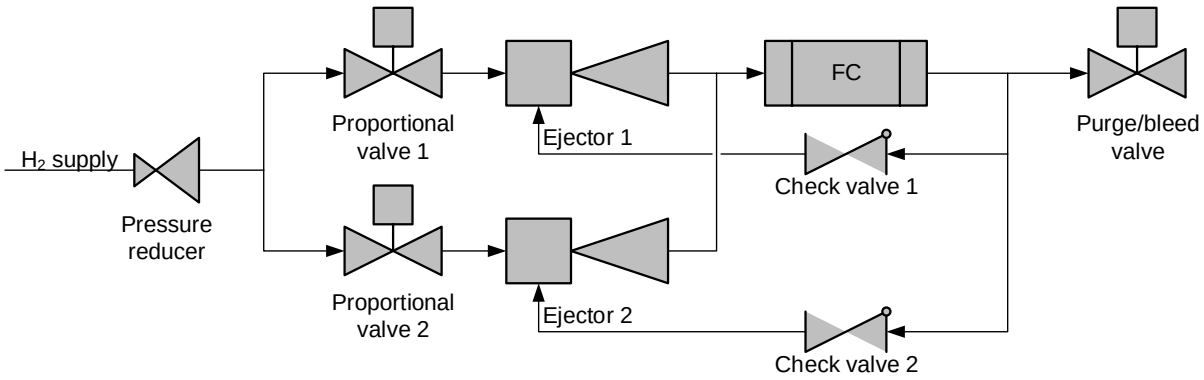

Figure 15. A schematic diagram of the target fuel cell system.

The ejectors are sized for the operating conditions listed in Table 4. The fuel cell stack inlet pressure (pFC,in = pe,out, ejector outlet pressure) is independent of the achieved recirculation rate. The fuel cell outlet pressure (i.e. the ejector secondary inlet pressure, ps,in) is varied to match the pressure in fuel cell.

The hydrogen and nitrogen dry gas mole fractions at fuel cell outlet are constant, 70% and 30% respectively. Also the fuel cell outlet temperature and relative humidity are constant, 75 °C and 100% respectively. However, the fuel cell outlet water mole fraction is not constant but varies

This project has received funding from the Fuel Cells and Hydrogen 2 Joint Undertaking under grant agreement No 779606. This Joint Undertaking receives support from the European Union's Horizon 2020 research and innovation programme, Hydrogen Europe and Hydrogen Europe research.

with fuel cell outlet pressure, which depends on fuel cell inlet pressure and fuel cell pressure drop. The pressure drop is a function of mass flow rate per cell:

$$\Delta p_s[bar] = p_{FC,in} - p_{FC,out} = 886.16 \cdot \frac{\dot{m}_{FC,in}\left[\frac{kg}{s}\right]}{N_{cell}} + 0.000188 \quad (1)$$

The pressure drop between fuel cell outlet and ejector secondary inlet is assumed negligible:

$$\Delta p_s[bar] \approx \Delta p_e[bar] = p_{e,out} - p_{s,in} \quad (2)$$

This project has received funding from the Fuel Cells and Hydrogen 2 Joint Undertaking under grant agreement No 779606. This Joint Undertaking receives support from the European Union's Horizon 2020 research and innovation programme, Hydrogen Europe and Hydrogen Europe research.

Table 4. Target fuel cell system operating conditions (specified by Powercell).

I_{stack}	$p_{FC,in}$	$y_{H2,FC,out,dry}$	$y_{N2,FC,out,dry}$	$T_{FC,out}$	$RH_{FC,out}$	λ_{target}
[A]	[barg]	[-]	[-]	[°C]	[%]	[-]
20	0.41	0.70	0.30	75	100	3.9
58.5	0.41	0.70	0.30	75	100	2.0
97.5	0.43	0.70	0.30	75	100	1.8
136.5	0.60	0.70	0.30	75	100	1.6
195	0.93	0.70	0.30	75	100	1.6
234	1.20	0.70	0.30	75	100	1.6

The maximum supply pressure (i.e. the pressure between the pressure reducer and the proportional valves) is assumed 10 barg.

4.2 Sizing method

The dual-ejector sizing can be divided into two parts: 1) sizing the nozzles and 2) sizing rest of the ejector dimensions. Nozzle sizing is conducted first since rest of the ejector dimensions depend on it.

Sizing of nozzles

The nozzles were sized so that they always operate with a primary pressure as low as possible but at or above critical conditions. This is because the ejector performance is known to improve when lowering the primary pressure (down to a primary pressure where a relatively rapid performance decrease begins) and to be more stable and less sensitive to disturbances when operated at super critical conditions [2]. The critical limit (when flow in nozzle reaches sonic limit) occurs when the primary pressure is above the critical limit, $p^*_{p,in}$:

$$p^*_{p,in}[bara] = p_{s,in}[bara] \cdot \left(\frac{2}{\gamma+1}\right)^{\frac{\gamma}{1-\gamma}} \quad (3)$$

where γ is the isentropic expansion factor. For hydrogen, $\gamma = 1.4$.

The nozzle sizing equation for super critical flow is [2]:

$$\dot{n}_{p,in} \times M_{w,p} = C \times \pi \left(\frac{D_{nt}}{2}\right)^2 \times p_{p,in}[bara] \times 10^5 \times \sqrt{\gamma \times \frac{M_{w,p}}{R \times (T_{p,in}+273.15)} \times \left(\frac{2}{\gamma+1}\right)^{\frac{\gamma+1}{\gamma-1}}} \quad (4)$$

This project has received funding from the Fuel Cells and Hydrogen 2 Joint Undertaking under grant agreement No 779606. This Joint Undertaking receives support from the European Union's Horizon 2020 research and innovation programme, Hydrogen Europe and Hydrogen Europe research.

where the molar primary gas flow rate is:

$$\dot{n}_{p,in} = \frac{I \cdot N_{cell}}{2 \cdot F} \quad (5)$$

The smaller ejector is designed to start operation at 20 A stack current. At this operating point, critical nozzle flow is achieved with a primary pressure of $p_{p,in}$ = 1.67 barg and a nozzle throat diameter of D_{nt} = 0.66 mm.

The larger ejector nozzle is sized to achieve the target maximum primary flow rate together with the smaller ejector at $p_{p,in}$ = 7.5 barg. With a maximum supply pressure of 10 barg, this leaves 2.5 bar pressure loss in the control valve. The larger nozzle has a diameter of D_{nt} = 1.08 mm.

Sizing of rest of ejector dimensions

The brute-force search method is employed for sizing rest of the ejector dimension. This means that all possible combinations of selected parameters are modelled. Table 5 lists the parameters varied.

Table 5. Varied parameters in every operating point listed in Table 4 (note that conditions for 20 A and 58.5 A stack currents are identical).

Variable	*Value 1*	*Value 2*	*Value 3*	*Value 4*
$p_{p,in}$ *[barg]*	$\frac{3}{4} \cdot p^*_{p,in}$	$p^*_{p,in}$	$\frac{1}{2} \cdot (p^*_{p,in} + 7.5)$	7.5
$p_{s,in}$ *[barg]*	p_{out}	$\frac{1}{3} \cdot (2 \cdot p_{out} + p^0_{s,in})$	$\frac{1}{3} \cdot (p_{out} + 2 \cdot p^0_{s,in})$	$p^0_{s,in}$
L_{ne} *[x* D_{nt}*]*	1.8	3.6	5.4	7.2
D_m *[x* D_{nt}*]*	6	9	12	15
L_m *[x* D_{nt}*]*	16	32	48	64

$p^0_{s,in}$ = expected secondary inlet pressure with zero secondary flow rate based on previous simulations

All combinations of the parameters in Table 5 were simulated at all operating conditions listed in Table 4 (operating conditions for 20 A and 58.5 A stack currents are identical so these were simulated together). This would sum up to 10240 design points if the simulations were to be done for both ejectors separately. Luckily, the ejector performance depends only on the relative dimensions, not absolute dimensions. That is, two ejectors with all dimensions proportional to each other result in identical λ-Δp_e –curves (or Ω-Δp_e –curves).

Since the various versions of the larger ejector are direct scale-ups of the smaller ejector (all dimensions are scaled in proportion), only the smaller ejector needs to be simulated. Hence, only 5120 design points needed simulation. However, the two ejectors cannot be expected to perform identically (e.g. when operated with same pressures) since the larger gives a higher

This project has received funding from the Fuel Cells and Hydrogen 2 Joint Undertaking under grant agreement No 779606. This Joint Undertaking receives support from the European Union's Horizon 2020 research and innovation programme, Hydrogen Europe and Hydrogen Europe research.

absolute recirculation rate, which translates into a higher pressure loss in stack, and, hence, a shift in operating point.

To estimate ejector performance between simulated conditions, the simulated entrainment ratios ($\Omega = \dot{m}_{s,in}/\dot{m}_{p,in}$) versus stack pressure drop were fitted into 2nd order polynomials, as follows:

$$\Omega = a \cdot \Delta p_e^2 + b \cdot \Delta p_e + c \quad (6)$$

Then each of the constants in Eq. 6 were fitted against primary gas mass flow rate ($\dot{m}_{p,in}$) into 2nd order polynomials, as follows:

$$\frac{1}{a} = a_2 \cdot \dot{m}_{p,in}^2 + a_1 \cdot \dot{m}_{p,in} + a_0 \quad (7)$$

$$\frac{1}{b} = b_2 \cdot \dot{m}_{p,in}^2 + b_1 \cdot \dot{m}_{p,in} + b_0 \quad (8)$$

$$\frac{1}{c} = c_2 \cdot \dot{m}_{p,in}^2 + c_1 \cdot \dot{m}_{p,in} + c_0 \quad (9)$$

where the primary gas flow rate through one ejector is computed from the 'ejector current' (i.e. the ejector's primary gas, hydrogen, flow rate translated into stack current):

$$\dot{m}_{p,in} = \frac{I_e \cdot N_{cell}}{2 \cdot F} \cdot M_{w,H_2} \quad (10)$$

Eqs. 6 to 9 fit perfectly the simulated data with $R^2 > 0.99$.

The resulting nine constants per a unique combination of D_m, L_{ne}, L_m, and I_e were organized into a table. The table served as a collection of unique combinations of ejector dimension among which the search was performed.

When the constant for Eq. 6 are known, the combined entrainment ratio (Ω_t) achieved with the two ejectors can be found by solving the following set of equations:

$$\Omega_t = \frac{\dot{m}_{s,in,s} + \dot{m}_{s,in,l}}{\dot{m}_{p,in,s} + \dot{m}_{p,in,l}} \quad (11)$$

$$\Omega_s = \frac{\dot{m}_{s,in,s}}{\dot{m}_{p,in,s}} = a_s \cdot \Delta p_e^2 + b_s \cdot \Delta p_e + c_s \quad (12)$$

$$\Omega_l = \frac{\dot{m}_{s,in,l}}{\dot{m}_{p,in,l}} = a_l \cdot \Delta p_e^2 + b_l \cdot \Delta p_e + c_l \quad (13)$$

$$\Delta p_e = d \cdot \left(\dot{m}_{s,in,s} + \dot{m}_{s,in,l} + \dot{m}_{p,in,s} + \dot{m}_{p,in,l}\right) + e \quad (14)$$

The solution is a quadratic equation with respect to $\dot{m}_{s,in,t} = \dot{m}_{s,in,s} + \dot{m}_{s,in,l}$ from which the total entrainment ratio can be calculated using Eq. 10. Further, the result can be used for calculating the stack pressure drop (Eq. 13), with which the water mole fraction, and ultimately hydrogen and nitrogen mole fractions as well, can be computed. Finally, the recirculation rate in terms of hydrogen stoichiometry can be computed.

With the method presented, the two ejectors can be optimized with respect to discrete values of D_m, L_{ne}, and L_m for both ejectors and continuous values of I_e for the one of the ejectors (the other is calculated from the stack current).

The search for an optimum (minimum cost) with respect to I_e is performed with Matlab's *fminsearch*-function. The cost function, which is minimized, is the negative sum of entrainment ratios. Further, the cost function is increased if any primary pressure becomes subcritical or if

This project has received funding from the Fuel Cells and Hydrogen 2 Joint Undertaking under grant agreement No 779606. This Joint Undertaking receives support from the European Union's Horizon 2020 research and innovation programme, Hydrogen Europe and Hydrogen Europe research.

the I_e is out of limits (0 A to flow rate in corresponding to maximum primary pressure, 7.5 barg). The optimization flowchart is shown in Figure 16.

This project has received funding from the Fuel Cells and Hydrogen 2 Joint Undertaking under grant agreement No 779606. This Joint Undertaking receives support from the European Union's Horizon 2020 research and innovation programme, Hydrogen Europe and Hydrogen Europe research.

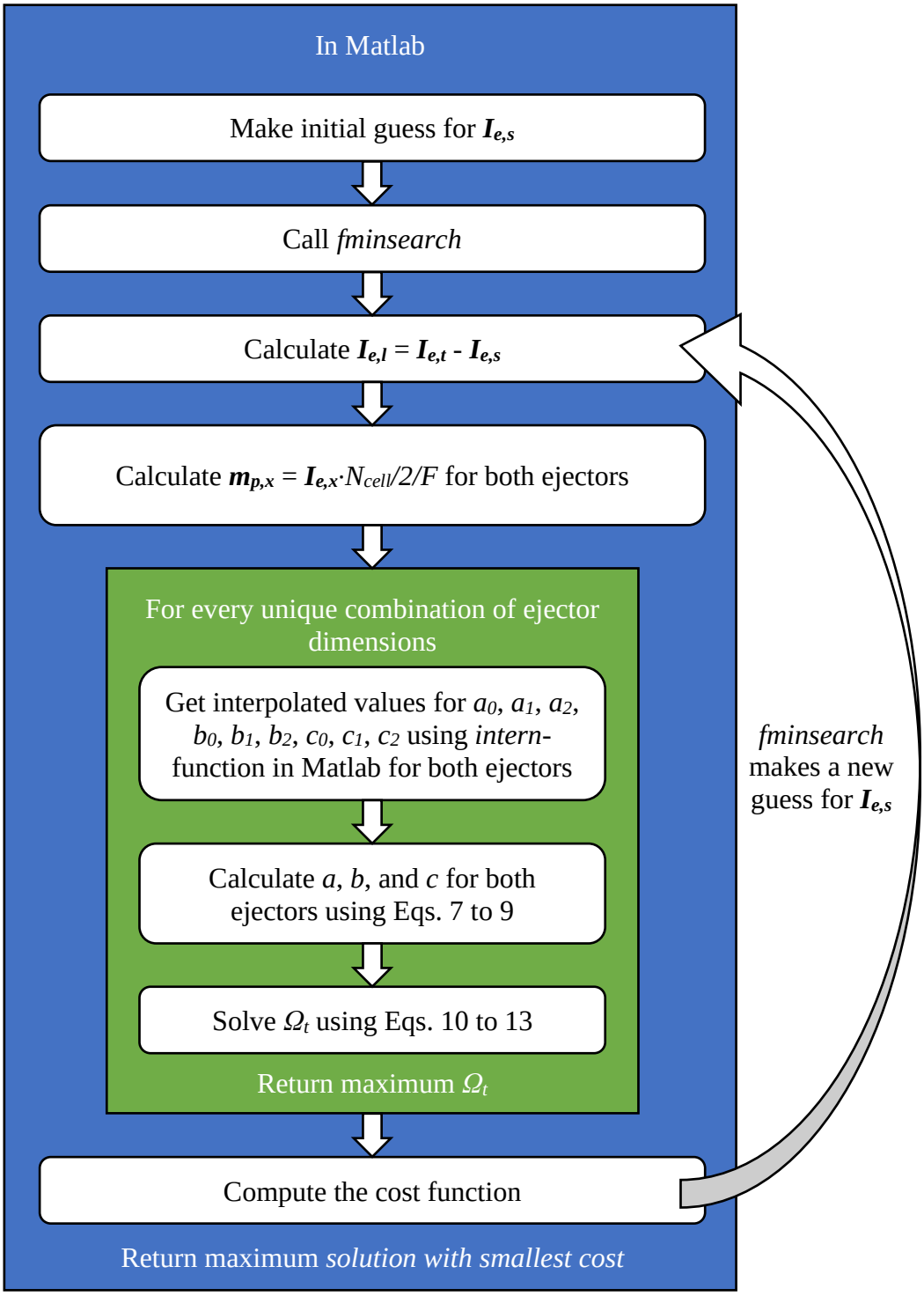

Figure 16. Optimization flow chart

It turns out that the search for optimum I_e split of flows between the ejectors can be simplified quite much. First, the larger ejector cannot be used at the I_{stack} = 20 A operating point, since the flow would be subcritical. Second, only one of the ejectors can be used at the I_{stack} = 58.5 A operating point, since the primary gas flow rate is not enough to achieve critical flow in both ejectors. Third (and finally), the primary gas pressure at the I_{stack} = 234 A operating point was

This project has received funding from the Fuel Cells and Hydrogen 2 Joint Undertaking under grant agreement No 779606. This Joint Undertaking receives support from the European Union's Horizon 2020 research and innovation programme, Hydrogen Europe and Hydrogen Europe research.

set to 7.5 barg for both ejectors at the design stage so the flow rates cannot be varied there. This leaves us with three 'continuous' variables (flow rate through the smaller ejector at operating conditions I_{stack} = 97.5, 136.5, 195 A) and one 'binary' variable (flow rate through the smaller ejector at operating condition I_{stack} = 58.5 A).

4.3 Results

The optimized ejector dimensions are shown in Table 6 and estimated performance of the ejectors are shown in Table 7.

Table 6. Optimized ejector dimensions.

Dimension	***Small ejector***	***Large ejector***
D_{nt}	0.66 mm	1.08
D_m	7.90 mm (= 12 x D_{nt})	9.71 (= 9 x D_{nt})
L_{ne}	3.55 mm (= 5.4 x D_{nt})	1.94 (= 1.8 x D_{nt})
L_m	21.1 mm (= 32 x D_{nt})	34.5 (= 32 x D_{nt})
α_d	5°	5°

Table 7. Estimated dual-ejector performance in the target system.

I_{stack} [A]	I_e [A]	$p_{p,in,s}$ [barg]	$p_{p,in,l}$ [barg]	$p_{s,in}$ [barg]	Ω_t [-]	Ω_s [-]	Ω_l [-]	λ [-]
20.0	20.0	1.67	-	0.404	31.5	31.5	0.0	3.7
58.5	58.5	6.84	-	0.395	27.0	27.0	0.0	3.3
97.5	43.5	3.62	2.13	0.411	19.5	7.6	11.9	2.7
136.5	63.4	5.40	3.42	0.574	19.7	7.2	12.5	2.8
195.0	63.4	7.50	5.55	0.893	19.4	6.0	13.5	2.9
234.0	63.4	7.50	7.50	1.155	19.6	3.5	16.1	3.0

Figure 17 shows the entrainment ratio with the optimized dual-ejector (blue curve) as function of stack current. The red curve shows the contribution of the smaller ejector. The contribution of the larger ejector is the area between these curves. The grey curve shows the target entrainment ratio.

This project has received funding from the Fuel Cells and Hydrogen 2 Joint Undertaking under grant agreement No 779606. This Joint Undertaking receives support from the European Union's Horizon 2020 research and innovation programme, Hydrogen Europe and Hydrogen Europe research.

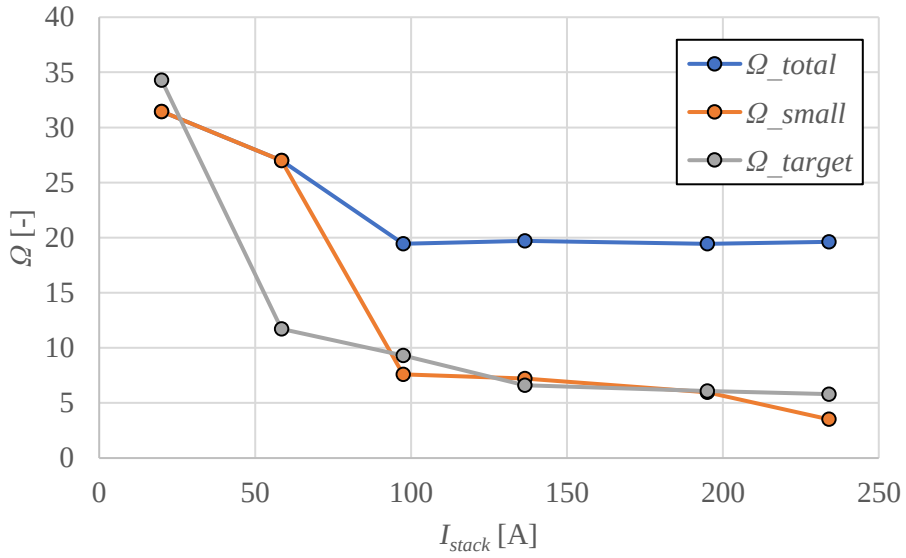

Figure 17. The entrainment ratio with the optimized dual-ejector (blue curve), the entrainment ratio with the optimized smaller ejector (red curve), and the target entrainment ratio (grey curve) as function of stack current.

Figure 18 shows the stoichiometric ratio with the optimized dual-ejector (blue curve) as function of stack current. The grey curve shows the target stoichiometric ratio.

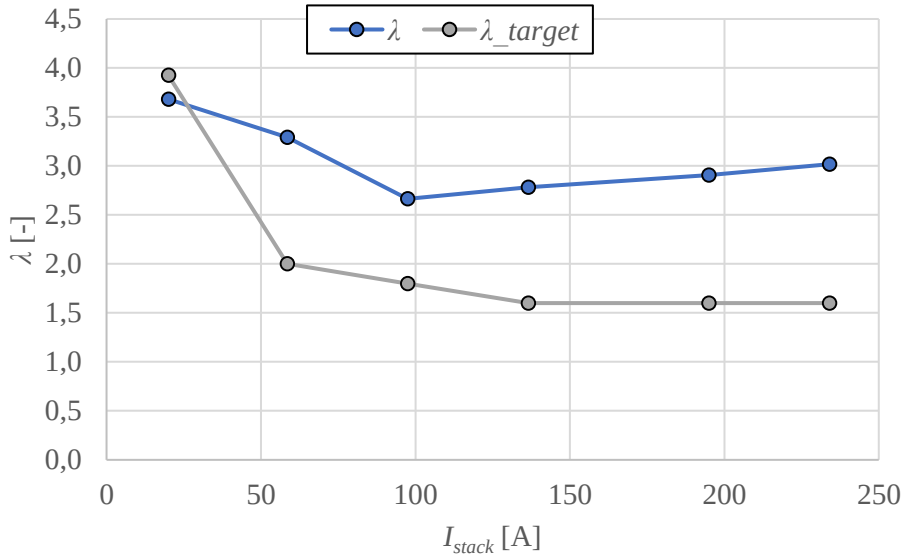

Figure 18. The hydrogen stoichiometric ratio with the optimized dual-ejector (blue curve) and the target stoichiometric ratio (grey curve) as function of stack current.

As seen in Figure 17 and Figure 18, the optimized dual-ejector seems to meet the target recirculation easily at most operating points. Only at the lowest stack current (I_{stack} = 20 A), the recirculation rate would be slightly below target. In this sense, the optimization can be regarded successful. This is much due to the low flow restriction of the stack.

This project has received funding from the Fuel Cells and Hydrogen 2 Joint Undertaking under grant agreement No 779606. This Joint Undertaking receives support from the European Union's Horizon 2020 research and innovation programme, Hydrogen Europe and Hydrogen Europe research.

However, as was shown in section 3.2, the simulations overestimate the ejector performance quite dramatically, especially at low current densities. Unfortunately, the ejector dimensions in the optimized dual-ejector are beyond those measured experimentally and modelled. The final experimental verification will reveal how well the dual-ejector performs.

This project has received funding from the Fuel Cells and Hydrogen 2 Joint Undertaking under grant agreement No 779606. This Joint Undertaking receives support from the European Union's Horizon 2020 research and innovation programme, Hydrogen Europe and Hydrogen Europe research.

5. Conclusion and Next steps

A dual-ejector system was designed and optimized based on three geometric parameters (mixing section diameter, mixing section length, and nozzle position relative to mixing section) and based on how the primary gas is divided between the two ejectors at various operating conditions. The brute-force optimization was based on a large number of simulations conducted with an axisymmetric 2D computation domain and with k-ε RNG turbulence model.

Based on optimization, the target recirculation is met with the dual-ejector system at almost every operating point. Only at the lowest stack current level, 20 A, the recirculation rate is slightly below target. The dual-ejector performance must, however, be verified experimentally before use in fuel cell system.

Experimental measurements were conducted with a modular ejector. The same ejector dimension that were the objective of optimization, were also varied in experiments. Experimental data showed that the mixing section diameter is the among the most important dimensions to optimize, besides the nozzle throat diameter.

The comparison of experimental data and simulation results show that the employed modelling method significantly overestimates ejector performance. Therefore, experimental verification of simulation results (such as the current optimized dual-ejector design) is always needed. Yet, the work on improving modelling accuracy will continue.

Finally, in this work, the dual-ejector system was optimized with respect to (only) three dimension. Even though some of these dimensions (the mixing section diameter in particular) might be among the most significant dimensions with regard to ejector performance other, less significant, dimension might have a notable effect also. There are numerous parameters to work with.

This project has received funding from the Fuel Cells and Hydrogen 2 Joint Undertaking under grant agreement No 779606. This Joint Undertaking receives support from the European Union's Horizon 2020 research and innovation programme, Hydrogen Europe and Hydrogen Europe research.

6. References

[1] Nikiforow, K., Pennanen, J., Ihonen, J., Uski, S., Koski, P. Power ramp rate capabilities of a 5 kW proton exchange membrane fuel cell system with discrete ejector control (2018) Journal of Power Sources, 381, pp. 30-37.

[2] Nikiforow, K., Koski, P., Karimäki, H., Ihonen, J., Alopaeus, V. Designing a hydrogen gas ejector for 5 kW stationary PEMFC system – CFD-modeling and experimental validation (2016) International Journal of Hydrogen Energy, 41 (33), pp. 14952-14970.

[3] Nikiforow, K., Koski, P., Ihonen, J. Discrete ejector control solution design, characterization, and verification in a 5 kW PEMFC system (2017) International Journal of Hydrogen Energy, 42 (26), pp. 16760-16772.

This project has received funding from the Fuel Cells and Hydrogen 2 Joint Undertaking under grant agreement No 779606. This Joint Undertaking receives support from the European Union's Horizon 2020 research and innovation programme, Hydrogen Europe and Hydrogen Europe research.